Delft University of Technology

Screening Approach for Identifying Cocrystal Types and Resolution Opportunities in Complex Chiral Multicomponent Systems

Li, Weiwei; De Groen, Mariette; Kramer, Herman J.M.; De Gelder, René; Tinnemans, Paul; Meekes, Hugo; Ter Horst, Joop H.

Important note
To cite this publication, please use the final published version (if applicable).
Please check the document version above.

Screening Approach for Identifying Cocrystal Types and Resolution Opportunities in Complex Chiral Multicomponent Systems

Weiwei Li, Mariette de Groen, Herman J. M. Kramer, René de Gelder, Paul Tinnemans, Hugo Meekes, and Joop H. ter Horst*

ACCESS | Metrics & More | Article Recommendations | SI Supporting Information

ABSTRACT: Cocrystallization of racemic-compound-forming chiral molecules can result in conglomerate cocrystals or diastereomerically related cocrystals, which enable the application of chiral separation techniques such as preferential crystallization and classic resolution. Here, a systematic method to identify the types and phase diagrams of cocrystals formed by chiral target compounds and candidate coformers in a particular solvent system is presented, which allows the design of suitable chiral resolution processes. The method is based on saturation temperature measurements of specific solution compositions containing both enantiomers of chiral molecules and a coformer. This method is applied to analyze three different systems. For racemic phenyl-

alanine (Phe) in water/ethanol mixtures one of the enantiomers selectively cocrystallizes with the opposite enantiomer of valine (Val), forming the more stable diastereomerically related cocrystal. The racemic compound ibuprofen crystallizes with the nonchiral coformer 1,2-bis(4-pyridyl)ethane (BPN) as racemic compound cocrystals. More interestingly, when it is combined with *trans*-1-(2-pyridyl)-2-(4-pyridyl)ethylene (BPE), the racemic compound ibuprofen cocrystallizes as a conglomerate, which in principle enables the application of preferential crystallization of this racemic compound. The systematic method shows the benefit of using pseudo-binary phase diagrams. Such pseudo-binary phase diagrams depict the saturation temperature on a very specific route through the quaternary phase diagram, allowing the identification of various cocrystal types as well as the corresponding cocrystallization conditions. The systematic method can be used to identify a suitable solid phase for chiral separation, and the obtained phase diagram information enables the performance of a crystallization-mediated chiral resolution process design. Such a guideline for a chiral resolution process design has never been reported for conglomerate cocrystal systems such as IBU:BPE, presented in this study.
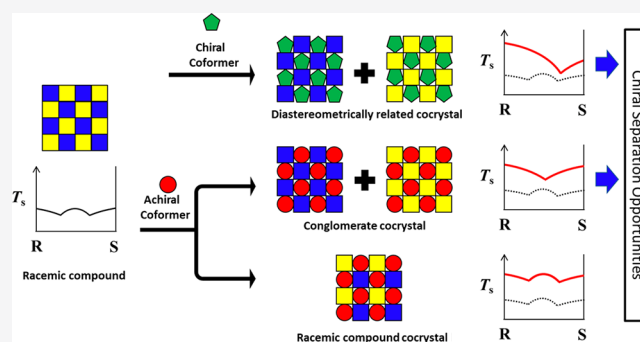
1. INTRODUCTION

Enantiomers of chiral products possess both pharmacological and toxicological differences. The awareness of such differences has driven the development toward new chiral separation techniques.[1,2] Chiral separation techniques such as preferential crystallization and Viedma ripening are now effective and efficient in achieving high enantiopurity for specific scientific examples of chiral products.[1,3−5] The general industrial application of these techniques requires the target compounds to form crystals which only contain a single enantiomer. However, in the substantial majority of the cases the two enantiomers of a chiral compound together form a solid (racemic compound), which significantly limits the application of chiral separation techniques.[6]

To overcome this drawback, various approaches can be followed to enable chiral separation through a solid-state conversion. A racemic-compound-forming chiral compound can be chemically modified into derivatives that crystallize as conglomerates. For instance, naproxen has been successfully

deracemized via its conglomerate ester derivatives.[7] Salt and solvate formation, for instance the ethanolamine salt of mandelic acid and the monohydrate of asparagine, can also provide the opportunity to convert a racemic compound to a conglomerate.[8−10] Alternatively, cocrystallization can modify the solid phase of target compounds for the application of separation techniques,[11−13] for instance by converting racemic compounds into conglomerate cocrystals for chiral separation.[14,15] Up until now, the conglomerate cocrystal systems of naproxen—nicotinamide and ibuprofen—*trans*-1-(2-pyridyl)-2-(4-pyridyl)ethylene (BPE) are the only two that have been reported in the literature.[16,17] Additionally, conglomerate

cocrystal hydrates, for instance the salicylic acid monohydrate of proxyphylline, have been reported.[18] Such cocrystal hydrate systems can also enable the chiral separation of racemic compounds,[19] but they will not be further discussed here, as the present study focuses on the binary system of chiral molecules and their coformers.

Various cocrystal types can be formed when a racemic compound and a coformer are combined into cocrystals. Cocrystals are crystals containing two or more neutral nonsolvent molecular components in the same crystal lattice.[20] Successful chiral coformers form two distinct diastereomerically related cocrystals with the enantiomers (see cocrystal type 1 in Scheme 1). The two enantiomers could be separated on

Scheme 1. Schematic Demonstration of Cocrystal Types Using a Racemic Compound (Blue and Yellow Squares) and a Chiral (Yellow Triangles) or Achiral (Red Circles) Coformer: (1) Diastereomerically Related Cocrystals; (2) Conglomerate Cocrystals; (3) Racemic Compound Cocrystals[a]

■ S-Enantiomer	● Achiral Coformer
■ R-Enantiomer	▲ Chiral Coformer
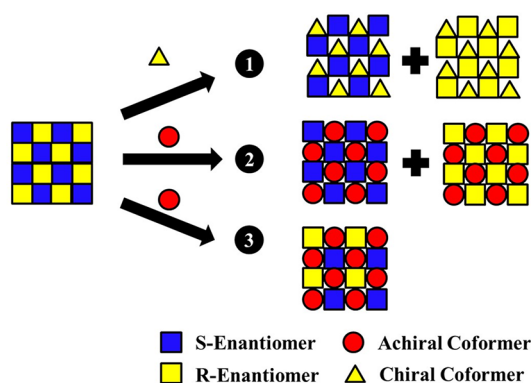
[a]For convenience we ignored the formation of relatively rare solid solutions.

the basis of solubility differences between diastereomeric cocrystals or between the cocrystals and the pure component crystals.[21,22] On the other hand, an achiral coformer can cocrystallize with a racemic compound into either a conglomerate or racemic compound cocrystals (see cocrystal types 2 and 3 in Scheme 1, respectively), and the former type paves the way to the application of chiral separation techniques such as preferential crystallization of the racemic compound via cocrystallization.[16,23] In much rarer cases, solid solution cocrystals are formed between an achiral coformer and a racemic compound, which contain random amounts of the two enantiomers in the lattice.[24] In the present study, solid solution cocrystals are not discussed due to their rarity. A systematic screening method to identify the various cocrystal types in these complex multicomponent chiral systems benefits the selection and design of a suitable chiral separation process.

The phase diagram of a multicomponent system provides information about the compositions in the various phases. However, a complete phase diagram for a quaternary system containing both enantiomers, a coformer, and a solvent, which also includes temperature as a variable, exists only in four-dimensional space. The construction of such a quaternary phase diagram requires large numbers of measurements, slowing down the efficient screening of suitable coformers for the target compound.[25] A projection of the interesting part of such a phase diagram on a two-dimensional plane, a pseudo-

binary phase diagram, can identify cocrystal formation as well as the cocrystal type with significantly fewer measurements and is thus suitable as a screening tool.

In this study, a systematic method using pseudo-binary phase diagrams is presented for identifying the cocrystal types formed using a racemic compound and a candidate coformer. The method has been experimentally verified as a useful screening procedure prior to the design and operation of a cocrystallization-mediated chiral separation process.

2. EXPERIMENTAL SECTION

2.1. Materials. Racemic ibuprofen (RS-IBU, 99%) and trans-1-(2-pyridyl)-2-(4-pyridyl)ethylene (BPE, 98%) were obtained from Santa Cruz Biotechnology. (S)-Ibuprofen (S-IBU, 99%), 1,2-bis(4-pyridyl)-ethane (BPN, 99%), heptane (99%), (S)-phenylalanine (S-Phe, ≥99.0%), (R)-phenylalanine (R-Phe, ≥ 98.0%), (RS)-phenylalanine (RS-Phe, ≥99.0%), (R)-Vvaline (R-Val, ≥98.0%), (S)-valine (S-Val, ≥98.0%), (RS)-valine (DL-Val, ≥99.0%), and ethanol were supplied by Sigma-Aldrich. All chemicals were used without further purification. The molecular structures of Val, Phe, IBU, BPN and BPE are shown in Figure 1.
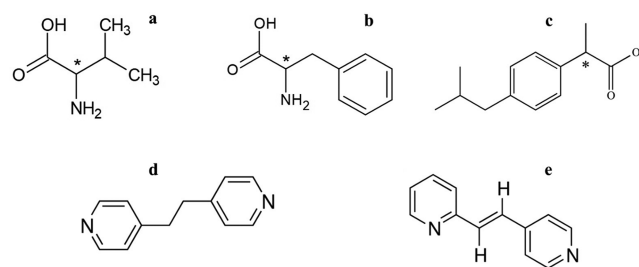

Figure 1. Molecular structures of Val (a), Phe (b), IBU (c), BPN (d) and BPE (e). Asterisks in (a)−(c) show the locations of the chiral centers.

From this point onward we will adopt the RS notation for the amino acids, meaning that D-Phe corresponds to R-Phe and D-Val corresponds to R-Val. This is done for consistency in notation throughout the paper.

2.2. Solubility Measurements. Crystal16 equipment (Technobis BV) was used for all saturation temperature measurements in this study, following a method developed by ter Horst et al.[26] A suspension of a known composition x was prepared from the pure components and the corresponding solvent. The suspension was linearly heated (0.3 °C/min) until full dissolution (clear point) and then linearly cooled (−0.3 °C/min) for recrystallization. The clear point temperature was noted as the saturation temperature T_s of the corresponding composition. The heating−cooling cycle was repeated three times, and the average T_s value was taken to represent the saturation temperature of the sample composition.

2.3. Saturation Temperature of Mixed Compositions. A series of mixed samples were prepared containing the target compound (either its racemic form or the enantiopure form) and the coformer in order to determine cocrystal existence. The compositions of the target compound (A) and the coformer (B) in the mixed samples were their equilibrium molar fractions $x_A^*(T_r)$ and $x_B^*(T_r)$ in the corresponding pure component solutions at various reference temperatures T_r, estimated from the van 't Hoff equation (eq 2). The measured $T_s(x_A^*(T_r),x_B^*(T_r))$ values of the mixed samples were compared with the T_r value. Positive temperature differences $\Delta T = T_s - T_r$ indicate the appearance of a solid different from either pure compound A or B. Due to the possibility of nonideal solutions, we assigned an arbitrarily chosen $\Delta T > 10$ °C to indicate the existence of a stable cocrystal consisting of compounds A and B.[26]

2.4. Type I Phase Diagram. In a type I phase diagram, the sample composition (x_A, x_B) of the target compound A (either its

Table 1. Molar Compositions of Samples for Each Type II Pseudo-Binary Phase Diagram[a]v

expt no.	target compound (A)	coformer (B)	solvent	x_A (mmol/mol)	x_B (mmol/mol)
1	RS-Val		ethanol/H_2O	7.6	0
2	RS-Phe		ethanol/H_2O	2.3	0
3	RS-Val	S-Phe	ethanol/H_2O	7.6	2.3
4	RS-Phe	S-Val	ethanol/H_2O	2.3	4.4
5	RS-IBU		heptane	114	0
6	RS-IBU	BPE	heptane	114	28
7	RS-IBU	BPN	heptane	114	28

[a]Abbreviations: A = target compound, B = coformer, Val = valine, Phe = phenylalanine, IBU = ibuprofen, BPE = *trans*-1-(2-pyridyl)-2-(4-pyridyl)ethylene, BPN = 1,2-bis(4-pyridyl)ethane. Ethanol/H_2O solvent composition: 20/80 v/v.

racemic form or enantiopure form) and the coformer B is described by the equation

$$\frac{x_B}{x_B*(T_r)} = 1 - \frac{x_A}{x_A*(T_r)} \tag{1}$$

where x_A and x_B are the molar fractions of the target compound (A) and the coformer (B), respectively, while x_A* and x_B* are the equilibrium molar fractions of A and B, respectively, at a chosen temperature T_r in their corresponding pure component solutions. The saturation temperatures T_s of such a series of samples were measured and plotted against the solvent-excluded molar fraction $y_B = x_B/(x_A + x_B)$, as a type I pseudobinary phase diagram.

2.5. TypeII Phase Diagram. In order to identify the racemic compound or conglomerate behavior of the cocrystals, a type II phase diagram was determined. In the samples of a type II phase diagram, the total molar fraction of both enantiomers $x_A = x_R + x_S$ is chosen constant, as well as the molar fractions x_B and $1 - x_A - x_B$ of coformer and solvent, respectively. This leaves the enantiomer fraction $y_S = x_S/(x_S + x_R)$ as a variable in the sample compositions. The measured saturation temperatures T_s for these samples with varying y_S values but constant x_B and x values were plotted against the molar fraction y_S of the S enantiomer in both enantiomers of the corresponding samples. The sample compositions used in all type II phase diagrams in the present study are shown in Table 1.

Two different solvent systems were used in the construction of type II pseudobinary phase diagrams. The selection of ethanol/H_2O, in the case of amino acid phase diagrams, was to avoid fouling and scaling, which usually took place when pure ethanol or water was used. Fouling and scaling negatively affect the accuracy of the solubility measurements. Heptane was used for the two systems from IBU, as it provided a solubility that was not too high for both racemic and enantiopure IBU, saving material and increasing the accuracy of the solubility measurements.

The composition ratio of the target amino acid and its coformer was decided by their corresponding single-component solubilities. Those between IBU and two other coformers were selected on the basis of trial and error, as the solubility of the coformers could not be precisely measured, partially because the coformer crystals were floating on top of the liquid surface, which caused significant fluctuation in the laser signal of Crystal16.

It should be noted that the solid phase is dissolved in the tests of constructing the phase diagrams. Therefore, the nature of the solid for which the solubility is determined is not known with explicit certainty. However, separate suspension tests allowed for confirmation of the presence of a cocrystal phase rather than the pure component crystal phases under conditions deduced from the phase diagrams.

2.6. X-ray Powder Diffraction (XRPD) to Identify the Crystalline Phase Composition. After recrystallization, samples were filtered at room temperature and the obtained solid was analyzed by XRPD, carried out with a Bruker D2 Phaser instrument (Bruker AXS GmbH, Karlsruhe, Germany). Data collection was done using monochromatic Cu Kα_1 radiation (λ = 0.154056 nm) in the 2θ region between 8 and 50°, with a 2θ step size of 0.022°. Data evaluation was done with the Bruker program EVA.

2.7. Construction of Theoretical Solubility Lines in the Type I and Type II Pseudo-Binary Phase Diagrams. In order to estimate the solubility in the various phase diagrams used, a modified van 't Hoff equation was used to account for solubility products:

$$\sum_i^N \ln x_i = -\frac{\Delta H}{R}\left(\frac{1}{T_s} - \frac{1}{T_0}\right) \tag{2}$$

where x_i are the molar fractions of the component(s) i, forming the solid phase, N is the total number of components i, including enantiomers, in the cocrystals, T_s (K) is the saturation temperature and ΔH and T_0 (K) are parameters specific for each solubility line and phase diagram, estimated from corresponding experimental data. As an example, the van 't Hoff parameters of the S-IBU–BPE cocrystal were estimated from the experimental T_s and the corresponding molar fraction product $x_{S-IBU} \cdot x_{BPE}$ values (N = 2 here, as R-IBU is not in the enantiopure cocrystal). In the case of the cocrystal of RS-IBU–BPN, on the other hand, the molar fractions of both R- and S-IBU and of BPN were taken into account. Therefore, ΔH and T_0 of RS-IBU–BPN were estimated from the experimental T_s and $x_{R-IBU} \cdot x_{S-IBU} \cdot x_{BPE}$ values (N = 3 here as both enantiomers and the coformer are in the cocrystals). The parameters of the van 't Hoff equation were used to interpolate or extrapolate the solubility of the target component at other temperatures, as well as to construct theoretical phase diagrams. It should be noted that the stoichiometry in the cocrystals is not taken into account in eq 2, as the phase diagrams are constructed prior to the structural determination of the cocrystals of interest (see the procedure detailed in the Discussion).

2.8. Single-Crystal X-ray Diffraction (XRD) of Cocrystals. Crystals of IBU–BPE suitable for X-ray diffraction were prepared by slowly evaporating an ethanol solution containing 510.3 mg/mL of RS-IBU and 232.0 mg/mL of BPE at 40 °C. For single-crystal X-ray diffraction a crystal was coated with high-viscosity oil, mounted on a Mitagen Microloop and shock frozen to 208 K using liquid nitrogen. Intensity data were collected at 208 K. The measurement was performed on a Nonius KappaCCD with φ and ω scans, using monochromated Mo Kα radiation.

Crystals of S-IBU–BPN suitable for X-ray diffraction were prepared by slowly evaporating an ethanol solution containing 19.9 mg/mL of S-IBU and 17.9 mg/mL of BPN at room temperature. For single-crystal X-ray diffraction, a crystal was coated with high-viscosity oil, mounted on a Mitagen Microloop, and shock frozen to 150 K using liquid nitrogen. Intensity data were collected at 150 K. The measurement was performed on a Bruker D8 Quest instrument with φ scans, using monochromated MoKα radiation.

The structures were solved using CRUNCH[27] (IBU–BPE) and SHELXT[28] (S-IBU–BPN) and were refined with standard methods using SHELXL.[29] All non-hydrogen atoms were refined with anisotropic temperature factors. The positions of the hydrogen atoms could initially be determined using a difference Fourier map. Hydrogens were subsequently, when possible, replaced by hydrogens at calculated positions and refined riding on the parent atoms. The S-IBU–BPN cocrystal structure with formula $C_{38}H_{48}N_2O_4$ refined to R1 = 0.0403 for 6486 reflections with $I_o > 2.0\sigma(I_o)$. The IBU–BPE cocrystal structure with formula $C_{25}H_{28}N_2O_2$ refined to R1 = 0.0397 for 5602 reflections with $I_o > 2.0\sigma(I_o)$.

3. RESULTS

3.1. Diastereomerically Related Cocrystals using Chiral Coformers.

Phenylalanine (Phe) and valine (Val) are amino acids with a single chiral center. Both amino acids are reported to crystallize as racemic compounds from racemic solutions. Interestingly, it has also been reported that S-Phe and R-Val can form a 1:1 cocrystal,[30] while to our knowledge there have been no reports on the diastereomerically related cocrystal with the same handedness of Phe and Val. Therefore, we chose to investigate the effect of the S-Val coformer for the RS-Phe system and the S-Phe coformer for the RS-Val system.

3.1.1. Pure Component Solubilities. First, the solubilities of the pure components S-Val, RS-Val, S-Phe, and RS-Phe in an 20%/80% v/v ethanol/water mixture were measured. The solubility is plotted as a function of temperature in Figure 2
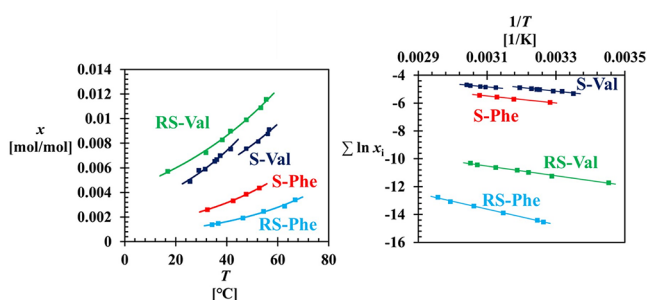
Figure 2. (left) Solubility of RS-Val, S-Val, RS-Phe, and S-Phe in 20%/80% v/v ethanol/water as a function of temperature. (right) The experimental data fitted to eq 2. The solid lines in both figures are theoretical solubilities estimated from eq 2.

(left) along with the corresponding van 't Hoff plots in Figure 2 (right). While the data points of the other compounds gave a good fit to eq 2, the solubility curve of S-Val showed a discontinuity near 42 mg/mL, which is possibly the result of S-Val polymorphism.[31] Since pure-component polymorphism is not the focus of this study, we did not look into this further. RS-Val shows a higher solubility in comparison to the enantiopure S-Val. At 50 °C, the solubility of S-Val is 44.5 mg/mL, which is more than half of the solubility of RS-Val at the same temperature (58.7 mg/mL), indicating that RS-Val is a racemic compound. RS-Phe shows a much lower solubility than S-Phe, which indicates that RS-Phe is a highly stable racemic compound. At 40 °C, the solubility of S-Phe is 25.7 mg/mL ($x_{\text{S-Phe}}^*(40\ °C) = 3.3$ mmol/mol) and the solubility of RS-Phe is 13.3 mg/mL ($x_{\text{RS-Phe}}^*(40\ °C) = 1.7$ mmol/mol). The experimental pure-component solubilities were fitted to eq 2 in order to determine the van 't Hoff parameters, which were used to estimate the phase diagrams of the model systems.

3.1.2. Saturation Temperatures of Cocrystal Systems. During a solution cocrystal screening, the composition with the highest possibility of forming a new cocrystalline material is not determined by the expected cocrystal stoichiometry but by the pure-component solubilities.[26] Specifically, a system containing the target compound A and the coformer B of the composition $[x_A^*(T_r), x_B^*(T_r)]$ has the highest possibility of forming cocrystals A−B, where x_A^* and x_B^* are respectively the equilibrium molar fractions of A and B at a reference temperature T_r.[26] If a more stable cocrystal forms, the measured saturation temperature $T_s > T_r$ of such a composition is usually substantially higher than the reference temperature T_r, since the saturation temperature T_s is that of

the more stable cocrystal rather than the pure-component crystals.[26]

Therefore, by measurement of the temperature difference $T_s − T_r$ new cocrystal materials constructed of the target molecule and the coformer can be identified.[26] Here the saturation temperatures of a series of mixtures of S-Phe, as the chiral coformer, and either S- or R-Val, as the target molecule, were measured. In Figure 3, the determined temperature difference
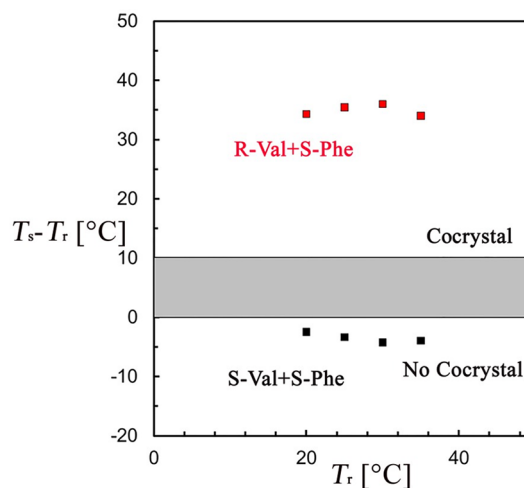
Figure 3. Difference $T_s − T_r$ between the saturation temperature T_s and reference temperature T_r of R-Val + S-Phe (red) and S-Val + S-Phe compositions (black) in 20%/80% v/v ethanol/water. The large positive difference (the region where $T_s − T_r > 10\ °C$, above the gray area) indicates the existence of a stable cocrystalline phase for R-Val:S-Phe, while there is no indication of a stable cocrystal from S-Val and S-Phe.

$T_s − T_r$ is plotted against the chosen reference temperature T_r. The saturation temperatures T_s of the R-Val:S-Phe system are substantially higher than the corresponding reference temperatures T_r, strongly indicating the existence of R-Val:S-Phe cocrystals. In contrast, the saturation temperatures of S-Val:S-Phe were slightly lower than the corresponding reference temperatures, suggesting that no cocrystallization took place between the two compounds.

3.1.3. Type I Pseudo-Binary Phase Diagrams. Chiral coformers interact differently with the opposite enantiomers of the same chiral compound. The results in Figure 3 suggest that Phe only cocrystallizes with Val of the opposite chirality and vice versa. For further verification, we investigated the saturation temperature behavior for three component mixtures of S-Val, with either S- or R-Phe in 20%/80% v/v ethanol/water.

At the top of Figure 4 the specific compositions are schematically indicated in a compositional pyramid of the quaternary system of the two enantiomers, coformer B, and solvent H. The red and green side triangles of the pyramid describe compositions of mixtures containing H, B, and one of the enantiomers of A following eq 1. On the target compound side the lines start at the pure component solubilities $x_R^*(T_r)$ and $x_S^*(T_r)$ at the reference temperature T_r. Both lines end at the pure component solubility $x_B^*(T_r)$ of the coformer B.

The lower left of Figure 4 shows the type I pseudobinary phase diagram of the target compound S-Val and the chiral coformer R-Phe in 20%/80% v/v ethanol/water. The type I phase diagram is divided into three parts by two eutectic
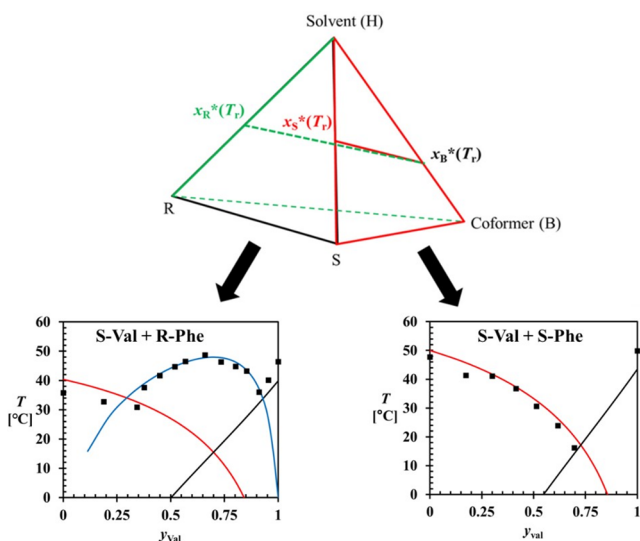
Figure 4. (top) Schematic demonstration of the compositional pyramid of a quaternary system of the target chiral compound consisting of enantiomers R and S, the coformer B, and the solvent H. The lines (either solid or dashed) crossing the red and green pyramid side planes represent the compositions of the type I pseudobinary phase diagrams from H, B, and one enantiomer of the target compound. (bottom) Type I pseudo-binary phase diagrams for the target enantiomer S-Val with coformer R-Phe at a reference temperature of 40 °C (left) and for the target enantiomer S-Val with coformer S-Phe at a reference temperature of 50 °C (right), both in a 20%/80% v/v ethanol/water mixture, showing the measured saturation temperatures T_s as a function of solvent-excluded molar fraction $y_{Val} = x_{Val}/(x_{Val} + x_{Phe})$. The molar compositions x_{Val} and x_{Phe} (for either S- or R-Phe) followed eq 1. Solid lines are predicted saturation temperatures of pure S-Val (black) and either S- or R-Phe (red) solutions from eq 2. The blue solid line is the theoretical saturation temperature of the cocrystal S-Val:R-Phe estimated from eq 2.

points. The two outer parts with decreasing saturation temperatures toward the middle indicate the saturation temperatures of solids of R-Phe and S-Val; the predicted saturation temperatures using the pure-component solubility results are represented by the red and the black solid lines, respectively. The middle part (0.3 < y_{Val} < 0.9), which significantly deviates from the theoretical saturation temperatures of the pure components, shows the composition region of the more stable cocrystal S-Val:R-Phe having higher saturation temperatures within that region.

The powder pattern of the collected crystals is distinctly different from those of both S-Val and R-Phe crystals. On the other hand, the powder patterns of the collected crystals and the reported[32] R-Val:S-Phe cocrystals are quite similar, despite strong preferential orientation in our powder sample (see details in the Supporting Information). Therefore, the formed solid phase of the samples in this middle region is indeed the cocrystal S-Val:R-Phe.

The type I pseudobinary phase diagram of the target compound S-Val and coformer S-Phe at the bottom right of Figure 4 shows that for the S-Val+S-Phe system no cocrystal region exists. The left part of the phase diagram indicates the solubility of S-Phe, the predicted saturation temperatures of which are represented by a red line. When y_{Val} > 0.7, where S-Val is theoretically the more stable solid phase, no saturation temperatures could be measured since none of the samples

recrystallized. It seems that S-Phe substantially inhibits the crystallization of S-Val.

A comparison between the two type I phase diagrams in Figure 4 and the results of the XRPD analysis show that Phe and Val can only form stable cocrystals with each other if they possess opposite chiralities.

3.1.4. Type II Pseudobinary Phase Diagram. A type II pseudo-binary phase diagram illustrates the change in solubility in a three- or four-component mixture in which only the ratio between the two enantiomers of the target chiral compound is varied. The shape of the phase diagram, especially the number and the location of its eutectic points, provides information about the types of the corresponding cocrystals[6] and the potential for chiral separation.

The top of Figure 5 shows the compositional pyramid of the quaternary system of the two enantiomers, coformer B, and
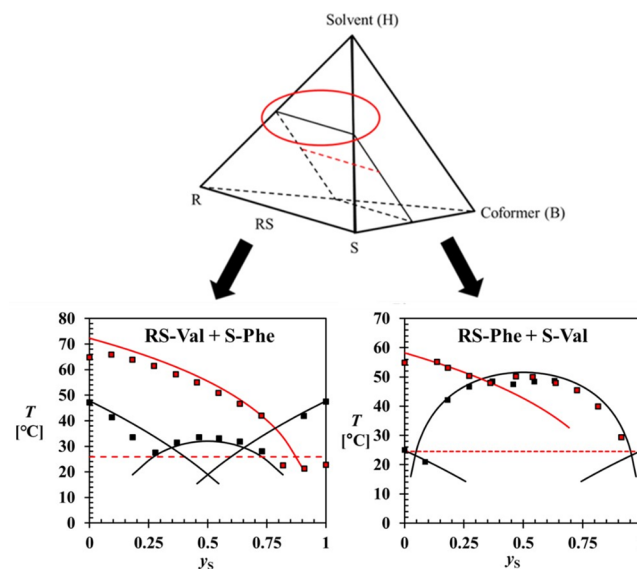

Figure 5. (top) Schematic demonstration of the compositional pyramid of a quaternary system of the target chiral compound consisting of enantiomers R and S, the coformer B, and the solvent H. The black line crossing the HRS plane and the red dashed line represent the compositions in type II pseudobinary phase diagrams of A in H, in the absence and presence of the coformer B, respectively. (bottom left) Type II pseudo-binary phase diagrams of RS-Val showing the saturation temperature T_s versus the enantiomer fraction y_S at x_{Val} = 7.6 mmol/mol in the absence (left, black) and presence of coformer S-Phe (x_{Phe} = 2.3 mmol/mol) (left, red). (bottom right) Type II pseudo-binary phase diagrams of RS-Phe (x_{Phe} = 2.3 mmol/mol) in the absence (right, black) and presence of the coformer S-Val (x_{Val} = 4.4 mmol/mol) (right, red) in a 20%/80% v/v ethanol/water mixture. The dashed lines indicate the predicted saturation temperature of the coformers. The black solid lines are predicted saturation temperatures T_s of Val (left) and Phe (right), estimated from eq 2. The red solid lines are theoretical T_s values of the cocrystal S-Phe:R-Val (left) and S-Val:R-Phe (right) estimated from eq 2 using the type I data.

solvent H. Through the black and red lines it shows the compositions for two type II pseudo-binary phase diagrams. The black line across the HRS plane represents the compositions of a constant total molar fraction of the target chiral compound and a varying R/S ratio in the absence of conformer B. The red dashed line in the interior of the pyramid represents the same total molar fraction of the target

chiral compound but now in the presence of a specific molar fraction of the coformer B.

3.1.5. RS-Val+S-Phe System. At the bottom left of Figure 5 two type II pseudo-binary phase diagrams of the target chiral compound Val in 20%/80% v/v ethanol/water in the absence (black) and presence (red) of the coformer S-Phe are shown. The measured saturation temperature T_s of each composition is plotted against the target compound S enantiomer fraction y_S = $x_S/(x_S + x_R)$ in the measured sample. On the outer sides (y_S < 0.3 and y_S > 0.7), the saturation temperatures represent the pure enantiomer crystals R-Val and S-Val, respectively. The symmetrical phase diagram shows two symmetrical eutectic points located around y_S = 0.3 and 0.7. Between the two eutectic points the racemic compound RS-Val is the more stable crystalline phase.

By addition of the coformer S-Phe (x_B = 2.3 mmol/mol), an asymmetrical type II pseudo-binary phase diagram is obtained in Figure 5 (left, red). This is because S-Phe only cocrystallizes with R-Val and not with S-Val. For the high y_S > 0.8, the saturation temperature of roughly 25 °C indicates that, instead of S-Val, S-Phe crystallized in the samples despite it being slightly less stable than S-Val. However, in a large region (0 < y_S < 0.8) of the phase diagram the elevated sample saturation temperatures are higher in the presence of coformer in comparison to those without the coformer, which shows that the cocrystal R-Val:S-Phe is more stable than both the RS-Val and R-Val crystal phases. The presence of the cocrystal in racemic Val solutions was confirmed with XRPD (see the Supporting Information). This indicates that, in a racemic Val solution containing the right amount of S-Phe, R-Val can selectively be separated by cocrystallization of the cocrystal R-Val:S-Phe.

3.1.6. RS-Phe+S-Val System. Similar to that of Val, the type II pseudo-binary phase diagram of Phe in Figure 5 (right, black lines) also contains two symmetrical eutectic points. Noticeably, since the solubility of RS-Phe is significantly lower than that of the pure enantiomer, the racemic Phe is the stable crystalline phase in a larger region in the phase diagram (0.1 < y_S < 0.9) in comparison to racemic Val.

In the presence of the coformer S-Val (4.4 mmol/mol) in the Phe system (Figure 5, right, red lines), the cocrystal R-Phe:S-Val is the most stable compound from y_S = 0 to y_S = 0.35. At a higher y_S, RS-Phe is the most stable compound. The powder pattern of the solid phase obtained from racemic Phe solutions in the presence of S-Val consists of a mixture of pure RS-Phe and cocrystal R-Phe:S-Val (see Figure SII in the Supporting Information). In order to obtain a pure R-Phe:S-Val cocrystal from racemic Phe solution,s the concentration of the coformer should be increased so that the cocrystal is stable under racemic conditions. In the type I phase diagram of R-Phe and S-Val (Figure 4, left bottom), the theoretical phase diagram of the cocrystal region gives the relationship between the saturation temperature T_s and the molar fraction product $x_{Phe} \cdot x_{Val}$ by using eq 2 and the values of parameter ΔH and T_0 from Table 2. In order to have a stable R-Phe:S-Val cocrystal whose saturation temperature T_s is higher than that of the pure RS-Phe solution (49 °C), the concentration of the coformer S-Val is estimated to be more than 6 mmol/mol, around 40% higher than the level present in the phase diagram in Figure 5 (right bottom).

3.2. Cocrystals using Achiral Coformers. Ibuprofen (IBU) is a commonly used nonsteroidal anti-inflammatory drug (NSAID), and S-IBU is over 100-fold more bioactive

Table 2. Values of the van 't Hoff Parameters in Eq 2 for Each Crystalline Material Introduced in This Study[a]

crystal composition	expt no.	ΔH (kJ/mol)	T_0 (K)
S-Val	1	21.5 ± 1.7	792 ± 177
S-Phe	2	19.7 ± 0.8	1314 ± 237
RS-Val	1	29.2 ± 1.1	363 ± 104
RS-Phe	2	46.8 ± 0.9	927 ± 85
R-Val-S-Phe or S-Val-R-Phe	3 and 4	43.4 ± 0.8	1209 ± 86
RS-IBU	5	134.7 ± 4.0	351 ± 18
S-IBU	5	58.4 ± 0.5	311 ± 4
S-IBU:BPE	6	55.3 ± 1.6	487 ± 28
RS-IBU:BPN	7	57.7 ± 3.4	576 ± 78
S-IBU:BPN	7	22.1 ± 2.4	1102 ± 430

[a]Abbreviations: Val = valine, Phe = Phenylalanine, IBU = ibuprofen, BPE = *trans*-1-(2-pyridyl)-2-(4-pyridyl)ethylene, BPN = 1,2-bis(4-pyridyl)ethane. The errors of the two parameters are standard deviations from fitting experimental data in the van 't Hoff equation.

than the R enantiomer.[33,34] RS-IBU crystallizes as a stable racemic compound, and Figure 6 shows that the solubility of
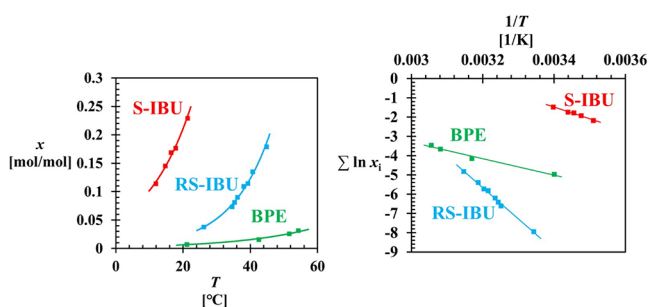

Figure 6. (left) Solubilities of RS-IBU, S-IBU, and BPE in heptane as a function of temperature. (right) Summations of the natural logarithms of equilibrium molar fractions x_i of each compound i are linear functions of the inverse of temperature T. The solid lines are a linear regression of the experimental data points.

the racemic IBU is significantly lower than that of its pure enantiomer in heptane. To investigate the cocrystal phase diagram behavior of RS-IBU and achiral coformers, two achiral coformers, BPN and BPE, were screened to identify their cocrystal types.

3.2.1. IBU:BPN Cocrystal. Solubility data of the achiral coformer BPN in heptane could not be reproducibly obtained from saturation temperature measurements because of the severe fluctuation of light transmission signals, probably from the crystals floating on the liquid−air interface in the vials. However, a rough estimate of the coformer BPN in heptane was obtained to be less than 5 mg/mL at room temperature.

As reliable solubility data of the coformer are not available, a short-cut approach was employed to quickly determine the type of cocrystals formed from IBU and BPN. In this short-cut approach, two heptane mixtures were prepared, one containing RS-IBU + BPN and the other S-IBU + BPN. In both mixtures, the concentrations of RS-IBU and S-IBU were 180 mg/mL and the BPN concentration was chosen to be 40 mg/mL. The saturation temperature of the RS-IBU + BPN mixture is around 49 °C, and that of S-IBU + BPN is approximately 40 °C. The saturation temperatures of RS-IBU and S-IBU at a concentration of 180 mg/mL are around 36 and 12 °C, respectively. Therefore, the saturation temperature T_s of the mixtures from RS- and S-IBU are respectively 13 and 28 °C

higher than those of the pure IBU. Moreover, although the solubility of BPN is unknown, the different T_s values of the two mixtures, which contain equal concentrations of the coformer, indicates that these T_s values are not of the pure component BPN. Therefore, it is likely that the solid phases from these two mixtures contain cocrystals from IBU and BPN.

This indication of cocrystal formation is confirmed by an XRPD analysis of the solid phases recovered from the two mixtures at room temperatures (see details in the Supporting Information). The powder patterns of the solid phases from both mixtures are different from those of the pure components IBU and BPN, indicating that the solid phases are cocrystals. Additionally, the two XRPD patterns of the cocrystals are different from each other, suggesting that the IBU:BPN cocrystal system is a racemic compound system rather than a conglomerate system.

BPN and RS-IBU are reported to cocrystallize as a racemic compound (see the crystal structure in Figure 7, top).[35] We further obtained single cocrystals of S-IBU:BPN for single-
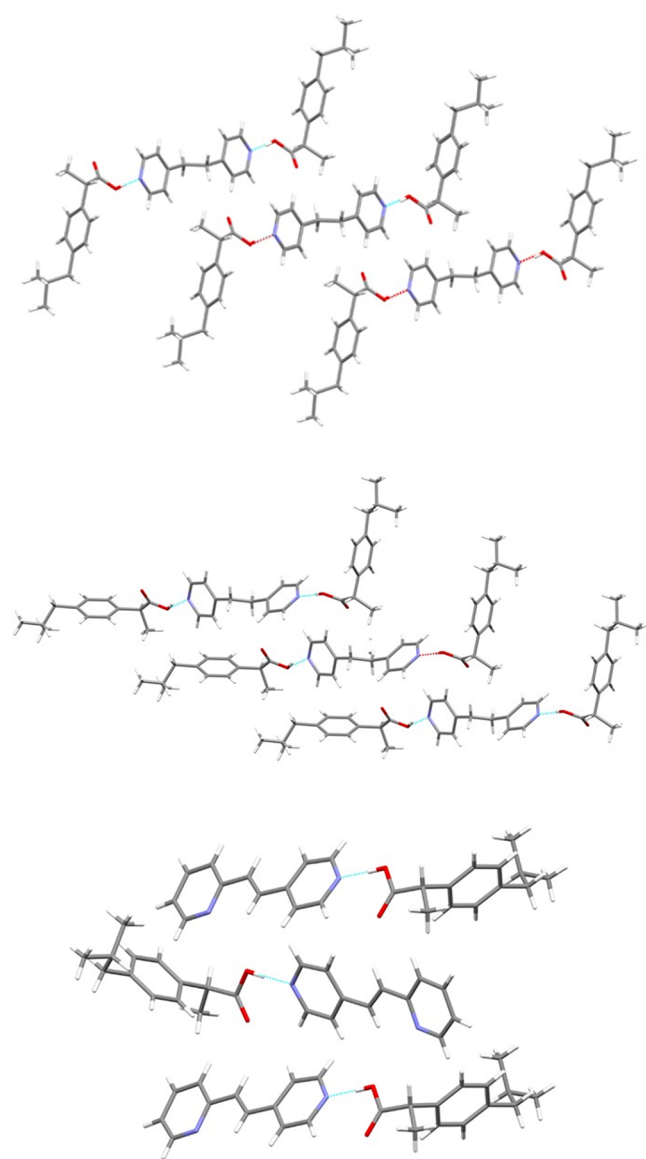
crystal XRD analysis. The obtained 1:2 S-IBU:BPN cocrystal structure is monoclinic with the space group $C2$ (No. 5) and unit cell parameters a = 18.2165(12) Å, b = 5.5960(4) Å, c = 33.393(2) Å, β = 92.075(2)°, and V = 3401.8(4) Å^3 and with Z = 4 asymmetric units in the cell. The asymmetric unit contains one molecule of BPN and two IBU molecules of S-IBU, leading to a 1:2 ratio for the two compounds BPN and S-IBU. The structure of the enantiopure IBU:BPN cocrystal is significantly different from that of the racemic cocrystal, which has a space group of $P\bar{1}$ (No. 2) and different dimensions of the unit cell (e.g., V = 853.26 Å^3).

An intermolecular hydrogen bond is formed between the hydroxyl groups of the IBU molecules and both nitrogen atoms at the pyridine groups of BPN (see structure in Figure 7, middle). The generated powder patterns from the racemic and enantiopure cocrystal structure data match those measured in the short-cut approach, indicating that the measured saturation temperatures T_s correspond to the solubilities of the cocrystals (see Figure SIII in the Supporting Information).

In a short-cut approach, the screening procedure stops when the single-crystal structure is obtained. However, one of the goals of this study is to demonstrate that the type II pseudo-binary phase diagrams of different types of cocrystals are distinctive, thus being feasible as a screening tool. Therefore, the type II pseudobinary phase diagram of the IBU:BPN system has been constructed and is shown in Figure 8.
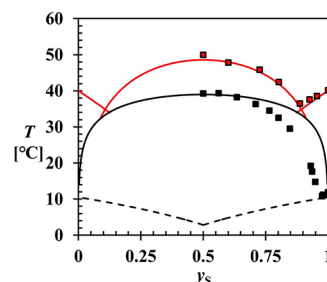

Figure 8. Type II pseudo-binary T_s, y_S phase diagrams of IBU (black) and IBU-BPN (red) in heptane. In both phase diagrams the total concentration of IBU was 180 mg/mL (x_{IBU} = 114 mmol/mol). In the IBU-BPN phase diagram (red) the concentration of the coformer BPN was 40 mg/mL (x_{BPN} = 28 mmol/mol). The points are saturation temperature measurements, and the lines are predicted from pure racemic compound solubilities (black solid line) and pure S- or R-IBU (black dashed line) as well as of cocrystals (red solid line) using eq 2.

The type II pseudo-binary phase diagram in the absence of the coformer (black) was constructed with a constant total concentration of 180 mg/mL IBU (x_{IBU} = 111 mmol/mol) and a varying S enantiomer fraction y_S. The phase diagram shows that IBU in heptane is a racemic compound system and the racemic form is significantly more stable than the pure enantiomer solid: the saturation temperature T_s of the racemic composition is approximately 30 °C higher than that of the pure R or S enantiomer.

The saturation temperatures between the two eutectic points, y_S = 0.05 and 0.95, are associated with the racemic compound RS-IBU. Enantiopure S- or R-IBU crystals can only be recovered from a system in which more than 95% of the IBU is composed of the corresponding enantiomer. The solubility lines of racemic IBU and the two enantiomers predicted from the pure compound solubilities in Figure 6 are

Figure 7. Structures of cocrystals RS-IBU:BPN (top),[35] S-IBU:BPN (middle), and enantiopure IBU:BPE (bottom).

shown as black solid lines in Figure 8 as well. Since the solubility of RS-IBU is significantly lower than that of either enantiomer, the racemic IBU is the dominant solid phase across a large part of the phase diagram. However, the measured phase diagram shows an increase in RS-IBU solubility in comparison to the predicted solubility: the presence of excess S enantiomer seems to influence the actual solubility toward higher values.

Figure 8 also shows the type II pseudo-binary phase diagram of 180 mg/mL (114 mmol/mol) IBU in the presence of a constant BPN coformer concentration of 40 mg/mL (x_{BPN} = 28 mmol/mol). The saturation temperature T_s at the racemic composition increased by approximately 15 °C, while that of the enantiopure form increased by more than 30 °C. Although the racemic form is still more stable within a large y_S range, the eutectic points moved closer toward the middle (from y_S = 0.05 and 0.95 to y_S = 0.1 and 0.9).

3.2.2. IBU:BPE Cocrystal. The solubility of the second achiral coformer, *trans*-1-(2-pyridyl)-2-(4-pyridyl)ethylene (BPE), is significantly lower than that of IBU. As can be seen from Figure 6 (left), at the same temperature, the solubility of RS-IBU is at least 4 times higher than that of BPE, while the S-IBU solubility is even higher (e.g., at 20 °C, solubilities of BPE, RS-IBU, and S-IBU are around 8, 35, and 370 mg/mL, respectively). Such a large solubility difference between the target compound A and the coformer B can lead to a type I pseudo-binary phase diagram with a eutectic point very close to one side due to the huge excess of IBU.

In order to verify cocrystal formation between IBU and BPE, saturation temperatures T_s of mixed RS-IBU and BPE samples in heptane were measured. In Figure 9 (left), the temperature
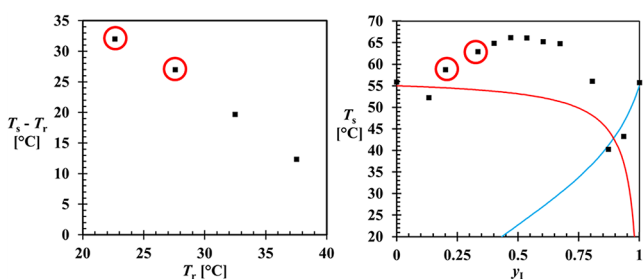
increasing IBU/BPE ratio, indicates the influence of the presence of IBU on the solubility of the cocrystals.

Furthermore, a type I pseudo-binary phase diagram is constructed from RS-IBU and BPE in heptane (Figure 9, right). The measured saturation temperatures T_s of mixtures of RS-IBU and BPE inheptane are plotted as a function of the solvent-excluded molar fraction y_{IBU} of RS-IBU. The increased saturation temperature T_s in the range $0.2 < y_{IBU} < 0.8$ indicates the existence of a cocrystal region. Further evidence for cocrystal formation is provided by the XRPD patterns from specific samples in this region (see Figure SIV in the Supporting Information), which indicate a solid phase different from those of the pure-component crystals. Interestingly, the maximum T_s of the cocrystal is not at the theoretical eutectic point of RS-IBU and BPE (y_I = 0.9 in Figure 9, right) but instead is at around the middle of the phase diagram. This observation is in line with that from Figure 9 (left), which suggests that the presence of an excess of IBU significantly increases the solubility of the cocrystals.

Following the confirmation of cocrystal formation between RS-IBU and BPE, a type II pseudo-binary phase diagram is constructed, in order to identify the cocrystal type. Saturation temperatures of samples with the same concentration of total IBU of 180 mg/mL (x_{IBU} = 114 mmol/mol) and BPE of 40 mg/mL (x_{BPE} = 28 mmol/mol) but varying enantiomer molar fraction $y_S = x_S/(x_S + x_R)$ are determined and plotted (red) in the phase diagram in Figure 10. The phase diagram (black) of only IBU with the same total concentration is also shown in Figure 10 as a comparison.
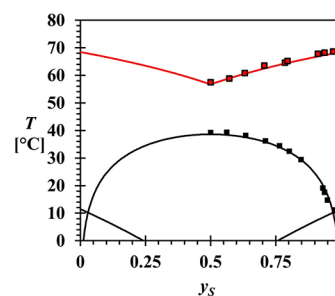

Figure 9. (left) The temperature difference ($T_s − T_r$) of samples with composition ($x_{RS\text{-}IBU}*(T_r), x_{BPE}*(T_r)$) versus the reference temperature T_r. (right) Type I pseudo-binary phase diagram of measured saturation temperature T_s as a function of the solvent-excluded molar fraction of RS-IBU $y_I = x_{IBU}/(x_{IBU} + x_{BPE})$ from RS-IBU-BPE mixtures in heptane. The molar compositions of $x_{RS\text{-}IBU}$ and x_{BPE} follow eq 1. The solid lines are theoretical saturation temperatures of pure RS-IBU (blue) and BPE (red) estimated from eq 2.

Figure 10. Type II pseudo-binary phase diagrams of IBU (x_{IBU} = 114 mmol/mol, black) and IBU:BPE (x_{IBU} = 114 mmol/mol and x_{BPE} = 28 mmol/mol, red) in heptane. The graph shows the saturation temperature T_s as a function of y_S, the molar fraction of the S enantiomer in total IBU. The red solid lines indicate the solubility of the enantiopure cocrystal R- or S-IBU-BPE, estimated from eq 2. The black solid lines are theoretical phase diagrams of pure-component IBU crystals.

differences $T_s − T_r$ of mixtures of RS-IBU and BPE in heptane were all substantial, which indicates the existence of the stable cocrystal IBU:BPE. In addition, the powder pattern (see the Supporting Information) of the solid phases collected for y_s = 0.5 indicate a solid phase different from IBU and BPE. It is noticeable in Figure 9 (left) that the temperature difference $T_s − T_r$ decreases as the reference temperature T_r increases. It can be seen from Figure 6 that BPE's solubility is significantly less sensitive to the temperature in comparison with IBU, which means that the increase in T_r in Figure 9 (left) is accompanied by a change in the sample solution stoichiometry of the two compounds. Therefore, the decrease in $T_s − T_r$, along with the

The type II pseudo-binary phase diagram of IBU and BPE in heptane in Figure 10 demonstrates a typical feature of a conglomerate system: only one eutectic point can be found at the racemic composition (y_S = 0.5) of the phase diagram. When the system is enriched with either enantiomer at the same total IBU concentration, the saturation temperature T_s is elevated. The estimated phase diagram (red solid line) also indicates the solubility of the enantiopure cocrystal. Two solid samples were taken at room temperature from the samples at y_S = 0.5 and 1 in Figure 10 and analyzed using XRPD. This shows that the crystalline phases from these two samples were mixtures of the same cocrystals with either the racemic or the enantiopure IBU (see Figure SV in the Supporting Information). These results strongly indicate that IBU and

Scheme 2. Schematic Isothermal Phase Diagrams of a Racemic Compound RS System without (Black Lines) or with (Red Lines) a Particular Amount of Coformer (either Chiral C or Achiral N)[a]
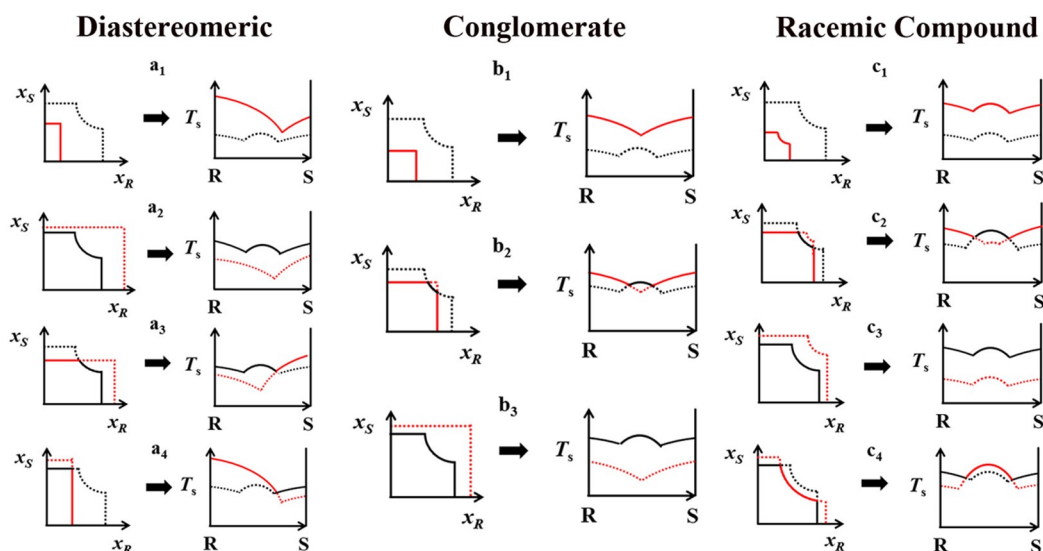
[a]On the right of the isothermal phase diagram the corresponding type II pseudo binary phase diagram is shown. The coformer can be chiral, leading to diastereomerically related cocrystal phases, or achiral, leading to conglomerate or racemic compound cocrystals. The solid lines indicate solubilities of the most stable compounds, while the dashed lines indicate those of the less stable compounds in the presence of the coformer.

BPE cocrystallize as conglomerates. Additionally, this conglomerate cocrystal system is special, as the racemic IBU is significantly more stable than its enantiopure IBU but its enantiopure cocrystal is more stable.

As a last step, single crystals were formed from racemic IBU and BPE in ethanol for cocrystal structure determination. The single cocrystal structure is monoclinic with the chiral space group $P2_1$ (No. 4), with unit cell parameters $a = 6.4896(2)$, $b = 9.5675(6)$, $c = 17.5232(10)$ Å, $\beta = 99.892(4)°$, and $V = 1071.83(10)$ Å^3 and with $Z = 2$ (see crystal structure in Figure 7, bottom). This structure is the same as that reported in the literature[17] and generates a simulated powder pattern that can be found back in the experimental patterns from the experiments in Figure 10 (see the Supporting Information for powder patterns). The single-cocrystal structure from the racemic IBU and BPE contains only one of the two IBU enantiomers; the system can thus be identified as a conglomerate cocrystal.

The asymmetric unit contains one molecule of BPE and one molecule of enantiopure IBU, leading to a 1:1 ratio for IBU and BPE. An intermolecular hydrogen bond is formed between the hydroxyl group of the carboxylic acid of the IBU molecule and the pyridine nitrogen at the four positions of BPE. IBU has $pK_a = 4.91$ while that of BPE can be estimated to be $pK_a = 5.5$, assuming a pK_a value equal to that of its structural isomer, *trans*-1,2-bis(4-pyridyl)ethylene,[36] indicating that cocrystals rather than salts are formed between the two compounds.

4. DISCUSSION

We have identified three different cocrystal types, a diastereomerically related cocrystal, a racemic compound cocrystal, and a conglomerate cocrystal, all formed from a racemic solution containing the coformer.

4.1. Cocrystal Variation. For each type of cocrystal, more composition possibilities exist and the corresponding isothermal and type II pseudo-binary phase diagrams are summarized in Scheme 2. In the isothermal phase diagrams,

the black lines show the solubility lines in a racemic compound system in the absence of coformer B (either chiral or achiral): the horizontal and vertical lines represent the equilibrium solution compositions in the case of a liquid−solid equilibrium between the solution and pure S and R crystals, respectively. The curved line shows the equilibrium solution composition in the case of a liquid−solid equilibrium between the solution and the racemic compound crystals. The intercept between the two straight lines and curved line indicates the eutectic composition at which a three-phase equilibrium exists among the solution, the racemic crystal, and the enantiopure crystal R or S. All red lines show the solubility lines of the same systems in the presence of a constant amount of B: the red solid lines indicate more stable solids and the red dashed lines less stable solids than those in the absence of B.

Similarly, in a type II pseudo-binary phase diagram, the black lines, solid or dashed, show the solubility of the target compounds, racemic or enantiopure, without the coformer B. In the presence of a coformer B at a constant molar fraction, a new liquid−solid equilibrium is established in the system, represented by a new phase diagram (red). The solid or dashed red lines indicate the solubility of crystals more or less stable than those without the coformer, respectively.

Phase diagrams a_1-a_4 demonstrate the equilibrium solution composition of diastereomerically related cocrystals R:B and S:B, such as the Phe-Val system. In a_1, both R:B and S:B cocrystals are more stable than the pure component crystals. Therefore, the red solid lines indicate the solubilities of the R:B and S:B cocrystals, which are different since the cocrystals are diastereomerically related. In a_2, both R:B and S:B cocrystals are less stable than the pure-component crystals. The solubilities of the more stable pure-component crystals are suggested by the black solid lines. In a_3, the S:B cocrystal is more stable than the S crystal but less stable than the RS crystal. Moreover, the R:B cocrystal is less stable than the pure-component crystals. The mixture of RS-Phe+S-Val in Figure 5 (right) is an example of a_3. In a_4, the R:B cocrystal is more

stable than both the RS and the R crystals but the cocrystals S:B are less stable than the S crystals. In this case, the phase diagram in the racemic or R enantiomer enriched region suggests the solubility of the R:B cocrystals, while the rest of the phase diagram indicates the solubility of the S crystals. A typical a_4 system is the RS-Val+S-Phe mixture in Figure 5 (left).

When an achiral coformer is used, the cocrystals formed are either conglomerates (type 2 in Scheme 1) or racemic compounds (type 3 in Scheme 1), with the rare exception of a solid solution. Phase diagrams b_1-b_3 show the phase behavior of conglomerate cocrystals S:B and R:B (type 2 in Scheme 1). The phase diagram b_1 describes the situation in which the enantiopure cocrystals are more stable than the pure RS crystals (such as in the case of RS-IBU+BPE system in Figure 10). Therefore, the phase diagram (red solid lines) suggests the solubilities of the two enantiopure cocrystals. In b_2, the RS crystals are still more stable than the enantiopure cocrystals in the region close to the racemic composition. Although the phase diagram with the coformer B (solid lines) is similar to the pure-component phase diagram, the parts on the two sides of the eutectic points (solid red lines) show the solubilities of the enantiopure cocrystals. In b_3, the cocrystals are less stable than the pure-component crystals. Therefore, the phase diagram with the presence of the coformer B is the same as that without.

Phase diagrams c_1-c_4 describe the phase behaviors of racemic compound cocrystals RS:B (type 3 in Scheme 1). In c_1, both the racemic cocrystals RS:B and the enantiopure cocrystals R:B and S:B are more stable than the pure-component crystals, for instance as in the case of the RS-IBU +BPN system in Figure 8. The phase diagram (solid red lines) suggests the solubilities of the cocrystals. In c_2, the enantiopure cocrystals are more stable than the S or R crystals but the RS crystals are still more stable than the cocrystals in the region close to the racemic composition. Therefore, the parts of the phase diagram on the two sides of the eutectic points (solid red lines) show the solubilities of cocrystal R:B or S:B while the region close to the middle indicates the RS crystal solubility. In c_3, the cocrystals are less stable than the pure-component crystals and the phase diagram with the coformer B is the same as that without. In c_4, the RS:B cocrystals are more stable than the corresponding pure-component crystals RS but the enantiopure R:B or S:B cocrystals are less stable than either R or S crystals. Therefore, the section between the eutectic points represents the solubility of the RS:B cocrystals, while the two sides indicate that of the enantiopure pure-component crystals R and S.

In addition to identifying cocrystal types, a type II pseudo-binary phase diagram also provides guidelines for the conceptual design of suitable chiral separation processes. Figure 5 gives suggestions on the chiral resolution of either Phe or Val. In the absence of the chiral coformer, the recovery of enantiopure Val or Phe cannot be achieved from their racemic solutions due to racemic compound formation. By addition of 18 mg/mL of the chiral coformer S-Phe, in a solution of Val (c_{Val} = 42 mg/mL), R-Val can be recovered in the form of R-Val:S-Phe cocrystals, even when the original solution is racemic. The cooling crystallization of R-Val:S-Phe can be operated until around 30 °C, which is the T_s value of pure RS-Val. Below this temperature, the nucleation of RS-Val can contaminate the cocrystal product. In the case of Phe, without the coformer S-Val, R-Phe can be recovered by cooling

crystallization if the solution is enriched so that $y_S < 0.1$. By addition of 24 mg/mL of the coformer S-Val, R-Phe can be recovered as R-Phe:S-Val cocrystals as long as the original solution has an enantiomeric excess $E > 0.4$ (corresponding to $y_S < 0.3$). It is estimated from eq 2 that, if the amount of S-Val increases to around 35 mg/mL of S-Val, R-Phe:S-Val cocrystals can be recovered from a racemic Phe mixture.

The achiral coformer BPN cocrystallizes with IBU as racemic compounds, which is not ideal for chiral separation techniques. However, the change in the position of the eutectic points can still reduce the requirement for the application of chiral separation: for instance, without cocrystallization, preferential crystallization could be applied on the IBU system if the solution is enriched with 95% of the S enantiomer, for instance by chiral chromatography.[37] With the coformer BPN, the requirement of enrichment is decreased to only 90%. Therefore, with a racemic compound cocrystal, a relatively less demanding chiral separation process can be designed.

4.2. Cocrystals for Resolution. With the structural information from the single crystal, IBU is confirmed to cocrystallize as a conglomerate using the coformer BPE. The IBU:BPE cocrystal is, to our knowledge, the second conglomerate cocrystal structure reported from a racemic compound, after the system of naproxen−nicotinamide.[16] The conversion from the racemic compound IBU to the conglomerate-forming IBU:BPE cocrystal enables the application of chiral separation techniques such as preferential crystallization. For instance, if a heptane solution of IBU, with a total concentration of 180 mg/mL, contained an initial enantiomeric excess E (e.g., E = 6%), a direct crystallization step could not recover an enantiopure solid phase, as can be seen from the phase diagram (black) in Figure 10. However, by addition of 40 mg/mL BPE into the system, the initial enantiomeric excess can all be recovered as enantiopure IBU:BPE cocrystals.

Although other cocrystals identified in this study are not conglomerates, they can still potentially be resolved. In the racemic solution in Figure 5 (left) there is sufficient chiral coformer present to make the enantiopure cocrystal compound more stable than the racemic compound. Under these conditions one enantiomer is selectively crystallized while the other remains in solution. In Figure 8 the racemic cocrystal is more stable than the racemic compound, resulting in a eutectic point shift which might enable integrated techniques such as chromatography and crystallization to be exploited.

Cocrystallization provides opportunities for the chiral separation of racemic-compound-forming molecules. Type II pseudo-binary phase diagrams can be used to identify the types of cocrystals from racemic compounds, as has been proven by the three systems investigated in this study. On the basis of this result, a systematic screening method has been developed to search for suitable cocrystal combinations of the target compounds for chiral separation opportunities. A demonstration of the newly developed screening method is shown in Scheme 3.

Stages I−III in the screening method are to identify the formation of cocrystals between the target chiral compound (A) and the selected coformer (B), as described by ter Horst et al. in a previous study on discovering new cocrystals.[26] The enantiomer of A is used if B is chiral and a racemic mixture of A is used if B is achiral.

In stage IV, the types of cocrystals are determined by a type II pseudo-binary phase diagram, single-crystal XRD (SCXRD)

Scheme 3. Screening Stages for Solids for Chiral Resolution Opportunities Based on the Phase Diagram Behavior of New Enantioselective Solids[a]
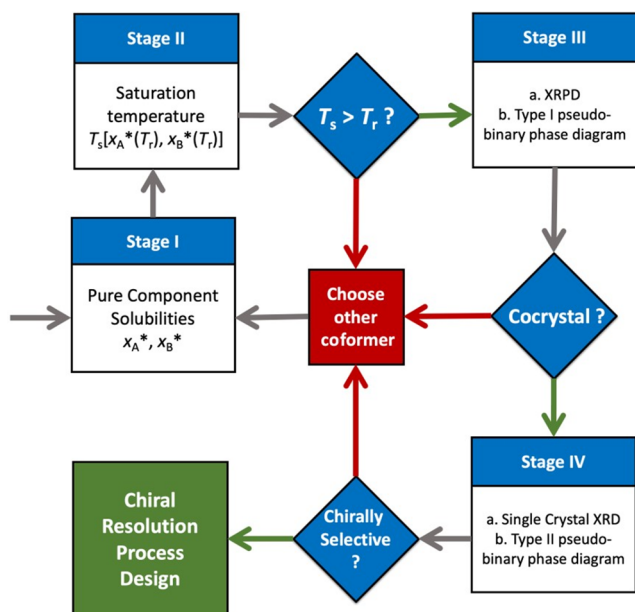
[a]In stage I the temperature-dependent pure component solubilities x_A^* and x_B^* of the target racemic molecule A and the coformer B are determined. In stage II, these solubilities at a series of particular reference temperature T_r are used to measure the saturation temperatures $T_s[x_A^*(T_r), x_B^*(T_r)]$ of the sample series with compositions $[x_A^*(T_r), x_B^*(T_r)]$. If $T_s > T_r$, it is likely a new, more stable solid has formed. In stage III XRPD or other solid-state analysis tools and phase diagram behavior from a type I pseudo-binary phase diagram will confirm cocrystal formation. The single-crystal XRD and type II pseudo-binary phase diagram in stage IV lead to information on the chiral selectivity potential for the new solid that can be exploited in a chiral resolution process design. Each question in the question box results in a yes (green arrow) or a no (red arrow).

or both. If applicable, the type II pseudo-binary phase diagrams (see the complete list of possible phase diagrams in Scheme 2) are used to select a suitable chiral separation technique for the target chiral compound.

In the case of B being an achiral coformer, a short-cut approach can be employed for quick screening, such as in the case of the IBU+BPN system in this study. Crystals can be formed from two solutions of compositions $[x_A^*(T_r), x_B^*(T_r)]$, where A is one enantiomer in one solution and is the racemic mixture in the other. The crystals from the two solutions are then analyzed by XRPD and the obtained powder patterns are first compared with those of pure-component crystals to determine whether cocrystals are formed. If so, the two XRPD patterns are compared with each other to determine whether conglomerate cocrystals are formed, as the patterns are the same from a conglomerate cocrystal system. In the case where solubility data are not available, two mixtures containing equal concentrations of one enantiomer and the racemic mixture of the target compound can be used. This short-cut procedure (see Scheme 3) determines whether or not the combination A−B forms the desired cocrystal types without the two pseudo-binary phase diagrams. As a tradeoff, relevant guidelines for chiral separation process design provided by type II pseudobinary phase diagrams are not available from the short-cut step.

In the pharmaceutical industry, in many cases, an undesired coformer might lead to toxicity of the drugs, which hinders the approval and the subsequent launch of these products. This imposes a potential challenge to the chiral resolution techniques mediated by cocrystallization. However, the coformer does not necessarily end up in the final formulation. In fact, such risks can be mitigated, if needed, via a suitable downstream process: e.g., recrystallization to separate the API from the coformer.[12]

5. CONCLUSIONS

A systematic phase-diagram-based screening method to identify the cocrystal types from racemic-compound-forming molecules has been developed and experimentally verified by studying three chiral systems. The system of Phe and Val in 20%/80% v/v ethanol/water mixtures forms diastereomerically related cocrystals. The nonchiral coformer BPN forms racemic compound cocrystals with IBU. The racemic compound IBU is converted into a conglomerate cocrystal by using the nonchiral coformer BPE. These three chiral compound systems have different type II pseudo-binary phase diagrams, which can be used to identify their cocrystal types and cocrystallization conditions. Such pseudo-binary phase diagrams enable a structured exploration of cocrystal phase diagrams of chiral compounds and their chiral separation opportunities.

■ ASSOCIATED CONTENT

Ⓢ Supporting Information

The Supporting Information is available free of charge at https://pubs.acs.org/doi/10.1021/acs.cgd.0c00890.

XRPD diffractograms of all relevant crystalline products from the present study (PDF)

Accession Codes

CCDC 1987385−1987386 contain the supplementary crystallographic data for this paper. These data can be obtained free of charge via www.ccdc.cam.ac.uk/data_request/cif, or by emailing data_request@ccdc.cam.ac.uk, or by contacting The Cambridge Crystallographic Data Centre, 12 Union Road, Cambridge CB2 1EZ, UK; fax: +44 1223 336033.

■ AUTHOR INFORMATION

Corresponding Author

Joop H. ter Horst − University of Strathclyde, EPSRC Centre for Innovative Manufacturing in Continuous Manufacturing and Crystallisation (CMAC), Strathclyde Institute of Pharmacy and Biomedical Sciences, Technology and Innovation Centre, Glasgow G1 1RD, United Kingdom; orcid.org/0000-0003-0118-2160; Email: Joop.terHorst@strath.ac.uk

Authors

Weiwei Li − Delft University of Technology, Department of Process and Energy, 2628 CB Delft, The Netherlands; orcid.org/0000-0001-8019-421X

Mariette de Groen − Delft University of Technology, Department of Process and Energy, 2628 CB Delft, The Netherlands

Herman J. M. Kramer − Delft University of Technology, Department of Process and Energy, 2628 CB Delft, The Netherlands; orcid.org/0000-0003-3580-8432

René de Gelder − *Radboud University, Institute for Molecules and Materials, 6525 AJ Nijmegen, The Netherlands;*
  ⊙ orcid.org/0000-0001-6152-640X

Paul Tinnemans − *Radboud University, Institute for Molecules and Materials, 6525 AJ Nijmegen, The Netherlands*

Hugo Meekes − *Radboud University, Institute for Molecules and Materials, 6525 AJ Nijmegen, The Netherlands;*
  ⊙ orcid.org/0000-0001-9236-2129

Complete contact information is available at:
https://pubs.acs.org/10.1021/acs.cgd.0c00890

Author Contributions

The manuscript was written through contributions of all authors. All authors have given approval to the final version of the manuscript.

Notes

The authors declare no competing financial interest.

■ REFERENCES

(1) Lorenz, H.; Seidel-Morgenstern, A. Processes To Separate Enantiomers. *Angew. Chem., Int. Ed.* **2014**, *53*, 1218−1250.

(2) Rouhi, A. M. Chirality at work. *Chem. Eng. News* **2003**, *81*, 56−61.

(3) Ward, T. J.; Ward, K. D. Chiral Separations: A Review of Current Topics and Trends. *Anal. Chem.* **2012**, *84*, 626−635.

(4) Coquerel, G., Preferential Crystallization. In *Novel Optical Resolution Technologies*, Sakai, K., Hirayama, N., Tamura, R., Eds.; Springer Berlin Heidelberg: Berlin, Heidelberg, 2007; pp 1−51.

(5) Sogutoglu, L.-C.; Steendam, R. R. E.; Meekes, H.; Vlieg, E.; Rutjes, F. P. J. T. Viedma ripening: a reliable crystallisation method to reach single chirality. *Chem. Soc. Rev.* **2015**, *44*, 6723−6732.

(6) Srisanga, S.; ter Horst, J. H. Racemic Compound, Conglomerate, or Solid Solution: Phase Diagram Screening of Chiral Compounds. *Cryst. Growth Des.* **2010**, *10*, 1808−1812.

(7) Noorduin, W. L.; Kaptein, B.; Meekes, H.; van Enckevort, W. J. P.; Kellogg, R. M.; Vlieg, E. Fast Attrition-Enhanced Deracemization of Naproxen by a Gradual In Situ Feed. *Angew. Chem., Int. Ed.* **2009**, *48*, 4581−4583.

(8) Li, W. W.; Spix, L.; de Reus, S. C. A.; Meekes, H.; Kramer, H. J. M.; Vlieg, E.; ter Horst, J. H. Deracemization of a Racemic Compound via Its Conglomerate-Forming Salt Using Temperature Cycling. *Cryst. Growth Des.* **2016**, *16*, 5563−5570.

(9) Spix, L.; Alfring, A.; Meekes, H.; van Enckevort, W. J. P.; Vlieg, E. Formation of a Salt Enables Complete Deracemization of a Racemic Compound through Viedma Ripening. *Cryst. Growth Des.* **2014**, *14*, 1744−1748.

(10) Wermester, N.; Aubin, E.; Pauchet, M.; Coste, S.; Coquerel, G. Preferential crystallization in an unusual case of conglomerate with partial solid solutions. *Tetrahedron: Asymmetry* **2007**, *18*, 821−831.

(11) ter Horst, J. H.; Cains, P. W. Co-Crystal Polymorphs from a Solvent-Mediated Transformation. *Cryst. Growth Des.* **2008**, *8*, 2537−2542.

(12) Urbanus, J.; Roelands, C. P. M.; Verdoes, D.; Jansens, P. J.; ter Horst, J. H. Co-Crystallization as a Separation Technology:

Controlling Product Concentrations by Co-Crystals. *Cryst. Growth Des.* **2010**, *10*, 1171−1179.

(13) Springuel, G.; Leyssens, T. Innovative Chiral Resolution Using Enantiospecific Co-Crystallization in Solution. *Cryst. Growth Des.* **2012**, *12*, 3374−3378.

(14) Harmsen, B.; Leyssens, T. Enabling Enantiopurity: Combining Racemization and Dual-Drug Co-crystal Resolution. *Cryst. Growth Des.* **2018**, *18*, 3654−3660.

(15) Guillot, M.; de Meester, J.; Huynen, S.; Collard, L.; Robeyns, K.; Riant, O.; Leyssens, T. Cocrystallization-Induced Spontaneous Deracemization: A General Thermodynamic Approach to Deracemization. *Angew. Chem., Int. Ed.* **2020**, *59*, 11303−11306.

(16) Neurohr, C.; Marchivie, M.; Lecomte, S.; Cartigny, Y.; Couvrat, N.; Sanselme, M.; Subra-Paternault, P. Naproxen−Nicotinamide Cocrystals: Racemic and Conglomerate Structures Generated by CO2 Antisolvent Crystallization. *Cryst. Growth Des.* **2015**, *15*, 4616−4626.

(17) Elacqua, E. *Supramolecular chemistry of molecular concepts:tautomers, chirality, Protecting groups, trisubstituted olefins, cyclophanes, and their impacton the organic solid state.* Ph.D. thesis, University of Iowa, Iowa City, IA, 2012.

(18) Harfouche, L. C.; Couvrat, N.; Sanselme, M.; Brandel, C.; Cartigny, Y.; Petit, S.; Coquerel, G. Discovery of New Proxyphylline-Based Chiral Cocrystals: Solid State Landscape and Dehydration Mechanism. *Cryst. Growth Des.* **2020**, *20*, 3842−3850.

(19) Harfouche, L. C.; Brandel, C.; Cartigny, Y.; Petit, S.; Coquerel, G. Resolution by Preferential Crystallization of Proxyphylline by Using Its Salicylic Acid Monohydrate Co-Crystal. *Chem. Eng. Technol.* **2020**, *43*, 1093−1098.

(20) Grothe, E.; Meekes, H.; Vlieg, E.; ter Horst, J. H.; de Gelder, R. Solvates, Salts, and Cocrystals: A Proposal for a Feasible Classification System. *Cryst. Growth Des.* **2016**, *16*, 3237−3243.

(21) Springuel, G.; Robeyns, K.; Norberg, B.; Wouters, J.; Leyssens, T. Cocrystal Formation between Chiral Compounds: How Cocrystals Differ from Salts. *Cryst. Growth Des.* **2014**, *14*, 3996−4004.

(22) Sánchez-Guadarrama, O.; Mendoza-Navarro, F.; Cedillo-Cruz, A.; Jung-Cook, H.; Arenas-García, J. I.; Delgado-Díaz, A.; Herrera-Ruiz, D.; Morales-Rojas, H.; Höpfl, H. Chiral Resolution of RS-Praziquantel via Diastereomeric Co-Crystal Pair Formation with l-Malic Acid. *Cryst. Growth Des.* **2016**, *16*, 307−314.

(23) Berry, D. J.; Seaton, C. C.; Clegg, W.; Harrington, R. W.; Coles, S. J.; Horton, P. N.; Hursthouse, M. B.; Storey, R.; Jones, W.; Friščić, T.; Blagden, N. Applying Hot-Stage Microscopy to Co-Crystal Screening: A Study of Nicotinamide with Seven Active Pharmaceutical Ingredients. *Cryst. Growth Des.* **2008**, *8*, 1697−1712.

(24) Chen, S.; Xi, H.; Henry, R. F.; Marsden, I.; Zhang, G. G. Z. Chiral co-crystal solid solution: structures, melting point phase diagram, and chiral enrichment of (ibuprofen)2(4,4-dipyridyl). *CrystEngComm* **2010**, *12*, 1485−1493.

(25) Reus, M. A.; van der Heijden, A. E. D. M.; ter Horst, J. H. Solubility Determination from Clear Points upon Solvent Addition. *Org. Process Res. Dev.* **2015**, *19*, 1004−1011.

(26) ter Horst, J. H.; Deij, M. A.; Cains, P. W. Discovering New Co-Crystals. *Cryst. Growth Des.* **2009**, *9*, 1531−1537.

(27) de Gelder, R.; de Graaff, R. A. G.; Schenk, H. Automatic determination of crystal structures using Karle-Hauptman matrices. *Acta Crystallogr., Sect. A: Found. Crystallogr.* **1993**, *49*, 287−293.

(28) Sheldrick, G. SHELXT - Integrated space-group and crystal-structure determination. *Acta Crystallogr., Sect. A: Found. Adv.* **2015**, *71*, 3−8.

(29) Sheldrick, G. Crystal structure refinement with SHELXL. *Acta Crystallogr., Sect. C: Struct. Chem.* **2015**, *71*, 3−8.

(30) Prasad, G. S.; Vijayan, M. X-ray studies on crystalline complexes involving amino acids and peptides. XXI. Structure of a (1:1) complex between l-phenylalanine and d-valine. *Acta Crystallogr., Sect. C: Cryst. Struct. Commun.* **1991**, *47*, 2603−2606.

(31) Moitra, S.; Kar, T. Growth and characterization of L-valine - a nonlinear optical crystal. *Cryst. Res. Technol.* **2010**, *45*, 70−74.

(32) Shiraiwa, T.; Ikawa, A.; Sakaguchi, K.; Kurokawa, H. Optical Resolution Of DL-Amino Acids With Aliphatic Side Chain By Using L-Phenylalanine. *Chem. Lett.* **1984**, *13*, 113−114.

(33) Nguyen, L. A.; He, H.; Pham-Huy, C. Chiral Drugs: An Overview. *Int. J. Biomed. Sci.* **2006**, *2*, 85−100.

(34) Chen, C. Y.; Chen, C. S. Stereoselective disposition of ibuprofen in patients with compromised renal haemodynamics. *Br. J. Clin. Pharmacol.* **1995**, *40*, 67−72.

(35) Alshahateet, S. F. Synthesis and Supramolecularity of Hydrogen-Bonded Cocrystals of Pharmaceutical Model Rac-Ibuprofen with Pyridine Derivatives. *Mol. Cryst. Liq. Cryst.* **2010**, *533*, 152−161.

(36) Shattock, T. R. *Crystal engineering of co-crystals and their relevance to pharmaceutical forms.* Ph.D. thesis, University of South Florida, Tampa, FL, 2007.

(37) Welch, C. J. Chiral Chromatography in Support of Pharmaceutical Process Research. In *Preparative Enantioselective Chromatography*; Cox, G. B., Ed.; Blackwell: Hoboken, NJ, 2005; pp 1−18.